ACS APPLIED MATERIALS & INTERFACES

Research Article

www.acsami.org

High-Performance Olivine $NaFePO_4$ Microsphere Cathode Synthesized by Aqueous Electrochemical Displacement Method for Sodium Ion Batteries

Yongjin Fang,[†] Qi Liu,[†] Lifen Xiao,[*,‡] Xinping Ai,[†] Hanxi Yang,[†] and Yuliang Cao[*,†]

[†]Hubei Key Laboratory of Electrochemical Power Sources, College of Chemistry and Molecular Sciences, Wuhan University, Wuhan 430072, China

[‡]College of Chemistry, Central China Normal University, Wuhan 430079, China

Supporting Information

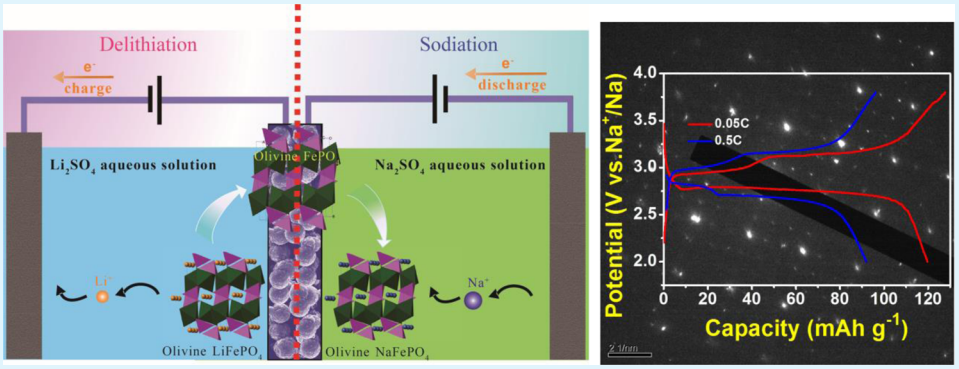

ABSTRACT: Olivine $NaFePO_4/C$ microsphere cathode is prepared by a facile aqueous electrochemical displacement method from $LiFePO_4/C$ precursor. The $NaFePO_4/C$ cathode shows a high discharge capacity of 111 mAh g^{-1}, excellent cycling stability with 90% capacity retention over 240 cycles at 0.1 C, and high rate capacity (46 mAh g^{-1} at 2 C). The excellent electrochemical performance demonstrates that the aqueous electrochemical displacement method is an effective and promising way to prepare $NaFePO_4/C$ material for Na-based energy storage applications. Moreover, the $Na_{2/3}FePO_4$ intermediate is observed for the first time during the Na intercalation process through conventional electrochemical techniques, corroborating an identical two-step phase transition reaction both upon Na intercalation and deintercalation processes. The clarification of the electrochemical reaction mechanism of olivine $NaFePO_4$ could inspire more attention on the investigation of this material for Na ion batteries.

KEYWORDS: *$NaFePO_4$, olivine structure, aqueous, electrochemical displacement, Na ion batteries*

1. INTRODUCTION

Rapid growth of renewable electricity requires low-cost electric energy storage (EES) devices for suppressing the impact of intermittent power on the electric grid. Although Li ion batteries (LIBs) are recognized as one of the most effective EES systems, concerns over the cost and continued availability of Li reserves have so far hindered its practical implementation for grid-scale energy storage application.[1−3] In this regard, Na ion batteries (SIBs), sharing a similar chemistry with LIBs, have attracted extensive investigation, due to the greater abundance and lower cost of Na resources compared to Li.[4−7]

A large variety of phases used in Li ion intercalation chemistry have been investigated as drop-in replacements for Na ion, including layered transition metal oxide O3- or P2-$NaMO_2$,[8−11] orthorhombic $Na_{0.44}MnO_2$,[12,13] phosphate polyanions,[14−20] and so on. Due to the much larger size, Na ion mobility in the cubic closed-packed oxide arrays is sluggish; the Na ion intercalation/deintercalation often results in very complicated phase transitions, leading to rapid structural degradation of the hosts upon cycling. From the structural point of view, open frameworks are more suitable to host the large-sized guest Na ions. For example, Prussian blue type materials have a cubic open framework capable of rapid and reversible Na ion movement, despite suffering from low specific capacity (about 100 mAh g^{-1}).[21−23] NASICON-type $Na_3V_2(PO_4)_3$, as one of the Na-superion conductors, has been demonstrated to have faster Na ion diffusion coefficient than its Li analogues.[19,24−26] Mixed transition metal maricite ($NaMn_{1/3}Co_{1/3}Ni_{1/3}PO_4$) has also been investigated as electrode materials and showed decent capacitor performance with 405 F g^{-1} over 1000 cycles.[27] However, the use of iron-based phosphates as host materials will be advantageous with regard to cost-effectiveness and environmental friendliness.[17,18,28,29] Among the series of iron phosphates, olivine

Received: May 29, 2015
Accepted: July 24, 2015
Published: July 24, 2015

DOI: 10.1021/acsami.5b04691
ACS Appl. Mater. Interfaces 2015, 7, 17977−17984

$NaFePO_4$ possesses the highest theoretical specific capacity (154 mAh g^{-1}) and decent working voltage, which make it attractive as a host material for Na ions.[28,30−32]

$NaFePO_4$ obtained from direct high-temperature synthesis usually presents a thermodynamically favored maricite phase, which has no free channels for Na ion diffusion in the closed framework.[18,33] Le Poul first found that the guest Li ions in the olivine iron phosphate host can be replaced by Na ions.[34] Afterward, olivine $NaFePO_4$ was frequently accessed via chemical or electrochemical displacement methods from olivine $LiFePO_4$ in organic solutions.[20,28,30−32] Oh et al. reported olivine $NaFePO_4$ prepared by electrochemical Li−Na exchange from $LiFePO_4$ with a stable capacity of 125 mAh g^{-1} at a current rate of 0.05 C.[28] Zhu et al. conducted a comparative study of the electrochemical performances of olivine $NaFePO_4$ in SIBs and olivine $LiFePO_4$ in LIBs and attributed the poorer performances of olivine $NaFePO_4$ to the lower diffusion coefficient of Na ions and higher charge transfer resistance in $NaFePO_4$ cathodes.[31] Meanwhile, the Na ion intercalation/deintercalation mechanism was thoroughly scrutinized.[35−37] Contrary to the direct biphasic reaction in micrometric $LiFePO_4$, a handful of research studies have found that Na ion intercalation/deintercalation underwent an intermediate phase close to $Na_{0.7}FePO_4$, which was recently identified to be an ordered $Na_{2/3}FePO_4$ composition.[32,35−38] The Na ion deintercalation from $NaFePO_4$ first went through a solid solution domain until the formation of $Na_{2/3}FePO_4$ phase and then proceeded through a two-phase process to form olivine $FePO_4$, which was characterized by two voltage plateaus on the charge profiles. The Na ion intercalation into olivine $FePO_4$ was reported to be different from the reversed Na ion deintercalation process.[32,35,36] Casas-Cabanas et al. reported the simultaneous existence of three phases: $FePO_4$, $Na_{2/3}FePO_4$, and $NaFePO_4$.[35,38] A single plateau was mostly observed on discharge profiles.[28,30−32,35,36,38] The asymmetric Na ion intercalation/deintercalation mechanism was generally ascribed to the larger volumetric mismatch between $NaFePO_4$ and $FePO_4$ (17.58% difference in unit volume) compared to only 6.9% for their Li counterparts.[35,38]

Previous works have shown that olivine $LiFePO_4$ can be reversibly (de)lithiated in aqueous solution, exhibiting fast diffusion kinetics as well as good cycling performance.[39,40] In aqueous SIBs, fast transport of Na ions has already been verified.[12,41,42] By analogy, it can be expected that $NaFePO_4$ could also undergo reversible sodiation in aqueous solution. Minakshi and Meyrick have shown that the maricite ($NaMn_{1/3}Co_{1/3}Ni_{1/3}PO_4$) is electrochemically active when using an aqueous NaOH electrolyte.[42] Recently, Vujković and Mentus reported a direct transformation from $LiFePO_4$ to $NaFePO_4$ in saturated $NaNO_3$ solution by cyclic voltammetry,[43] clearly proving the feasibility of electrochemical synthesis of $NaFePO_4$ via aqueous medium. Herein, we report a facile synthesis of olivine $NaFePO_4$ by aqueous electrochemical displacement of Li ions from olivine $LiFePO_4$ by Na ions. This displacement process is quick, easy, cost-saving, and green compared to that in organic electrolyte, and the thus-obtained $NaFePO_4$ cathode shows high reversible capacity and cycle performance in SIBs. Moreover, we reveal, for the first time, that the Na ion intercalation/deintercalation can proceed in a reversible two-step phase transition reaction and a clear phase separation is determined by reaction rate.

2. EXPERIMENTAL SECTION

2.1. Material Synthesis and Electrode Preparation. All of the reagents were purchased from Alfa Aesar without further purification. $LiFePO_4$/C microsphere precursor was prepared by a template-free hydrothermal process as described in our previous work:[44] Stoichiometric amounts of $CH_3COOLi{\cdot}2H_2O$, $Fe(NO_3)_3{\cdot}9H_2O$, $NH_4H_2PO_4$, and citric acid (mole ratio is 1:1:1:1) were dissolved in deionized water to form a transparent solution of 70 mL. The solution was then transferred into a 100 mL Teflon-lined stainless steel autoclave and maintained at 180 °C for 6 h. Afterward, the hydrothermal product was mixed with an appropriate amount of sucrose, dehydrated at 80 °C overnight, and then calcined at 650 °C for 10 h in a 5% H_2/Ar atmosphere to obtain the $LiFePO_4$/C microspheres.

The $LiFePO_4$ electrode was prepared by roll-pressing the thoroughly mixed paste of 80 wt % $LiFePO_4$/C, 10 wt % acetylene black, and 10 wt % polytetrafluoroethylene into a thin film (∼5 mg cm^{-2}) and pressing the film onto a Ti mesh.

The $NaFePO_4$ electrode was obtained by a two-step aqueous electrochemical transition process. The aqueous cell has a three-electrode design, with $LiFePO_4$ electrode (∼1 cm^2) as working electrode, activated carbon electrode as counter electrode, and Ag/AgCl electrode (0.197 V vs NHE) as reference electrode. The three electrodes were first inserted into 1 mol L^{-1} Li_2SO_4 aqueous solution and fully charged (delithiated) to 0.7 V with a current rate of 17 mA g^{-1}. Then, the three electrodes were thoroughly rinsed with deionized water, transferred into 1 mol L^{-1} Na_2SO_4 aqueous solution, and fully discharged (sodiated) to −0.6 V at a current of 17 mA g^{-1} to achieve an olivine $NaFePO_4$ electrode. The $NaFePO_4$ electrode was also rinsed with deionized water and dried at 70 °C in vacuum overnight for use.

2.2. Characterization. X-ray powder diffractions were obtained by using a Shimadzu XRD-6000 diffractometer with Cu Kα. The data were recorded in the 2θ range of 15−60° with a scan rate of 4° min^{-1} at a step size of 0.02°. The morphologies of the materials were observed by SEM (Merlin Compact FE-SEM, Zeiss) and TEM (JEM-2100F). The element dispersive spectroscopy (EDS) mapping of the composite was obtained from an oxford detector (X-Max^N, Oxford) attached to the SEM. The selected electron diffraction was obtained by TEM with the operated potential set at 200 kV. The carbon content in the $LiFePO_4$/C microspheres was analyzed by CHNS Vario EL cube (Elementar Analysen Systeme GmbH, Hanau, Germany).

2.3. Electrochemical Measurements in Organic Electrolyte. The electrochemical cells were assembled into CR2016-type coin cells, with $NaFePO_4$ electrode as cathode, Na thin disk as anode, cellgard 2035 as separator, and 1.0 mol L^{-1} $NaPF_6$ dissolved in ethylene carbonate/diethyl carbonate (EC/DEC, 1:1 by volume) as electrolyte. The cell assembly was carried out in a glovebox with water/oxygen content lower than 0.5 ppm, and the loading mass of the active material was ∼4 mg cm^{-2}. The room temperature constant current discharge/charge tests were conducted on a LAND cycler (Wuhan Kingnuo Electronic Co., Wuhan, China). Cyclic voltammetry measurements were performed on a CHI 660a electrochemical workstation (ChenHua Instruments Co., Shanghai, China).

3. RESULTS AND DISCUSSION

3.1. Synthesis and Characterization of the $NaFePO_4$/C Microsphere. $LiFePO_4$/C microsphere precursor was prepared by a template-free hydrothermal process as described in our previous work.[44] The SEM and TEM images of the product are shown in Figure 1. It shows that the product appears as micrometer-sized spheres with a quite uniform diameter of ∼3.5 μm (Figure 1a,c). The enlarged image of a single microsphere shows that it was composed of densely aggregated nanoparticles and has a porous structure (Figure 1b).This peculiar structure should favor electrolyte infiltration as well as obtain high tap density. The carbon content in the product was evaluated to be 2.8% by element analysis. The $LiFePO_4$/C microsphere electrode demonstrated excellent Li ion inter-

DOI: 10.1021/acsami.5b04691
ACS Appl. Mater. Interfaces 2015, 7, 17977−17984

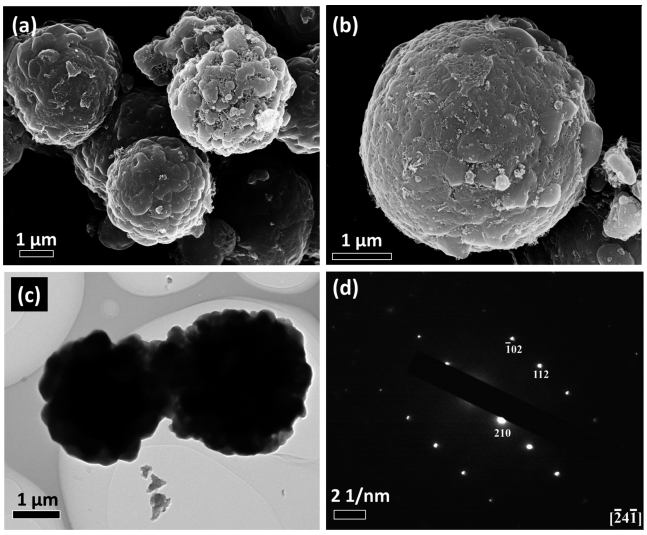

Figure 1. SEM (a and b) and TEM (c) images and SAED pattern (d) of the $LiFePO_4/C$ microspheres precursor.

calation/deintercalation electrochemical performance in both organic and aqueous systems as shown in Figure S1 (see Supporting Information (SI)), guaranteeing a highly structure-stable architecture to be used for making $NaFePO_4/C$.

The synthetic scheme of the olivine $NaFePO_4/C$ through an aqueous electrochemical displacement is illustrated in Figure 2.

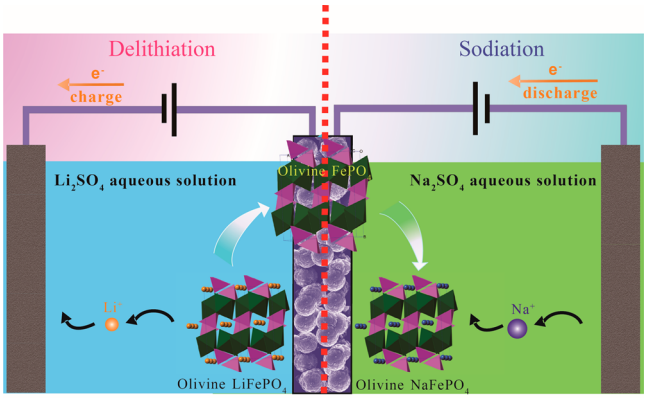

Figure 2. Synthetic scheme of the aqueous electrochemical displacement process from olivine $LiFePO_4$ to isostructural $NaFePO_4$.

First, the olivine $LiFePO_4/C$ electrode was fully delithiated (charged) in 1 mol L^{-1} Li_2SO_4 aqueous solution to get the isostructural $FePO_4/C$. After being washed thoroughly by deionized water, the $FePO_4/C$ electrode was transferred into 1 mol L^{-1} Na_2SO_4 aqueous solution and then fully sodiated (discharged) to obtain the final olivine $NaFePO_4/C$ electrode. The $NaFePO_4/C$ electrode was then vacuum-dried for use.

Parts a and b of Figure 3 present the cyclic voltammetry (CV) and constant current charge–discharge illustrations demonstrating the direct electrochemical conversion from $LiFePO_4/C$ to $NaFePO_4/C$ in aqueous solutions, respectively. The aqueous cell has a three-electrode design, with $LiFePO_4/C$ electrode as working electrode, activated carbon electrode as counter electrode, and Ag/AgCl electrode (0.197 V versus NHE) as reference electrode. Figure 3a gives the CV plots scanned at 1 mV s^{-1}. When first scanned positively in Li_2SO_4 aqueous solution from −0.3 to 0.7 V (denoted by blue solid

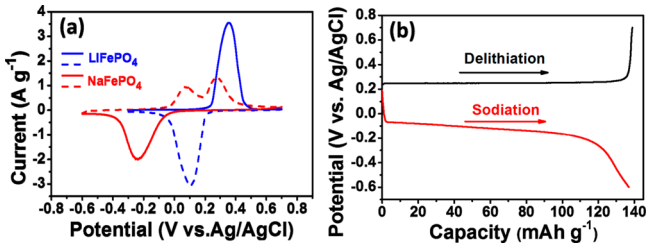

Figure 3. (a) Cyclic voltammetry and (b) constant current charge–discharge illustration of the aqueous electrochemical displacement process from olivine $LiFePO_4$ to $FePO_4$ in 1 mol L^{-1} Li_2SO_4 solution and then to $NaFePO_4$ in 1 mol L^{-1} Na_2SO_4 solution.

line), the electrode presents an intensive delithiation peak at 0.35 V. When the electrode was transferred into Na_2SO_4 aqueous solution and scanned negatively from 0.7 to −0.6 V (red solid line), a broad sodiation peak was observed at −0.25 V, exhibiting a successful displacement process of Li ions by Na ions. Figure 3a also gives the corresponding lithiation and desodiation processes as presented in dashed lines. The reversed lithiation of $FePO_4/C$ occurs at 0.1 V (the blue dashed line in Figure 3a), and the reversed desodiation of $NaFePO_4/C$ gives two peaks at 0.05 and 0.3 V (the red dashed line in Figure 3a). Based on the intervals of the redox peaks, it is apparent that $LiFePO_4$ shows faster reaction kinetics than $NaFePO_4$ in aqueous solution. Besides, the areas of the two desodiation peaks of $NaFePO_4/C$ are estimated to be about 1:2. Obviously, the CV feature of $NaFePO_4$ in aqueous solution is quite similar to that observed from organic solution in refs 31 and 43 and our work shown later, indicating that the reaction mechanisms of $NaFePO_4$ in aqueous and organic systems are identical. Thus, it can be reasonably speculated that the two desodiation peaks originate from a two-step reaction process and are sequentially attributed to the desodiation of $NaFePO_4$ to $Na_{2/3}FePO_4$ intermediate phase, and then to $FePO_4$.

Figure 3b gives the charge profile of the $LiFePO_4/C$ electrode in Li_2SO_4 aqueous solution and the discharge profile in Na_2SO_4 aqueous solution cycled at 0.1 C (1 C = 170 mA g^{-1} based on $LiFePO_4$). The $LiFePO_4/C$ electrode presents a typical flat delithiation voltage profile at 0.25 V with a capacity of ca.140 mAh g^{-1}, and a sloping sodiation plateau at −0.1 V with a capacity of 137 mAh g^{-1}, suggesting that almost all interstitial sites originally occupied by Li ions are taken over by Na ions through one discharge–charge process. SEM (Figure 4a,b,e) and TEM (Figure 4c) observation further revealed that the obtained $NaFePO_4/C$ composites retained a microspherical structure. The corresponding elemental mappings of Na, Fe, P, and O are shown in Figure 4f–i, exhibiting a uniform element distribution in the microsphere. The EDS spectrum (Figure 4j) analysis shows that the Na/Fe/P/O ratio is nearly 1:1:1:4, indicating that the microsphere is $NaFePO_4$.

What's more, Figure 5 gives the XRD patterns of the initiative $LiFePO_4$ samples fully charged to 0.7 V in Li_2SO_4 aqueous solution and fully discharged to −0.6 V in Na_2SO_4 aqueous solution. As can be seen, all of the XRD reflections can be well-indexed to a pure olivine phase respectively, indicating a very robust olivine framework constituted by $FePO_4$. Thus, Figures 4 and 5 confirm that $LiFePO_4$ can be successfully transformed into $NaFePO_4$ through a two-step aqueous electrochemical process.

3.2. Electrochemical Measurement of the $NaFePO_4/C$ Microsphere in Organic Electrolyte. The olivine $NaFePO_4/$

DOI: 10.1021/acsami.5b04691
ACS Appl. Mater. Interfaces 2015, 7, 17977–17984

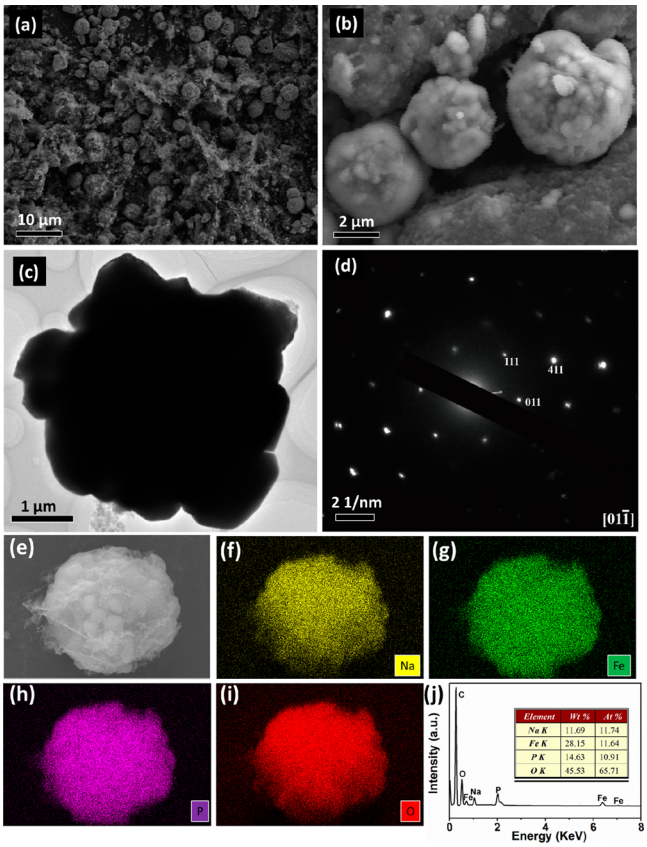

Figure 4. SEM (a and b) and TEM (c) images and SAED pattern (d) of the $NaFePO_4$/C microspheres converted electrochemically in aqueous solution; (e) typical SEM image of as-prepared $NaFePO_4$/C microsphere and the corresponding elemental mapping of sodium (f), iron (g), oxygen (h), and phosphorus (i), and EDS spectrum of the $NaFePO_4$/C microsphere (j; inset, element content of the mapping area).

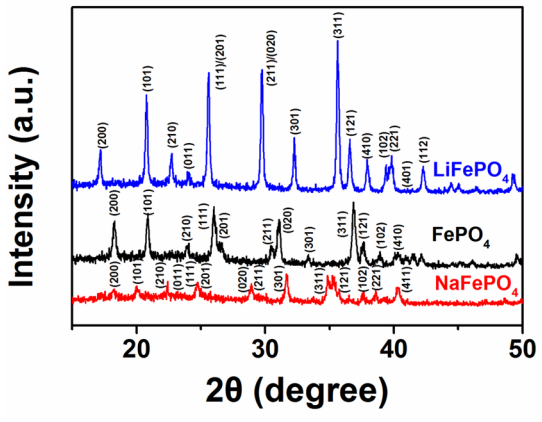

Figure 5. XRD patterns of the pristine $LiFePO_4$/C powder, the fully delithiated $FePO_4$/C electrode in 1 mol L^{-1} Li_2SO_4 aqueous solution, and the final sodiated $NaFePO_4$/C electrode in 1 mol L^{-1} Na_2SO_4 aqueous solution.

C electrode prepared by aqueous electrochemical displacement was assembled into coin cells with Na electrode and 1 mol L^{-1} $NaPF_6$/EC:DEC (1:1 by volume) electrolyte. The electrochemical test results of the $NaFePO_4$/C electrodes are presented in Figure 6. The CV curve scanned at a rate of 0.05 mV s^{-1} in Figure 6a shows two well-defined desodiation

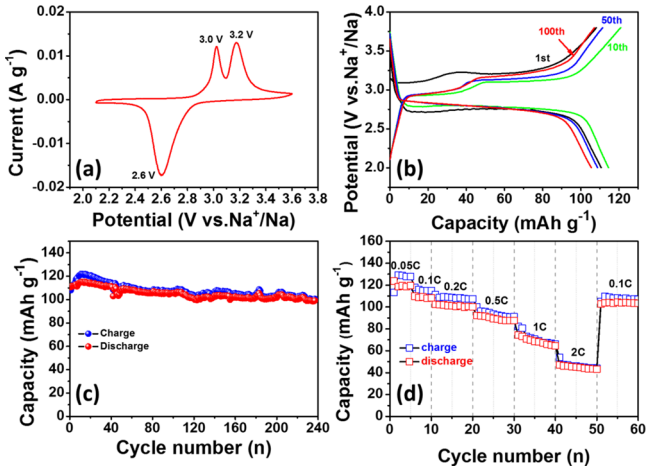

Figure 6. Electrochemical performance of the $NaFePO_4$/C cathode: (a) Cyclic voltammogram scanned between 2.1 and 3.6 V vs Na^+/Na at a rate of 0.05 mV s^{-1}; (b) constant current charge/discharge profiles and (c) charge/discharge capacity versus cycle number at 0.1 C; (d) rate cycling performance at various rates from 0.05 to 2 C. The counter electrode was a Na disk electrode, and the electrolyte was 1.0 mol L^{-1} $NaPF_6$/EC:DEC (1:1 by volume); the voltage window of charge/discharge was 2.0−3.8 V.

peaks and a single sodiation peak, in good accord with those reported in previous study.[31,43] Figure 6b shows the charge−discharge profiles at different cycles at a current rate of 0.1 C (1 C = 154 mA g^{-1}). Over 100 cycles, two charge plateaus at 2.90 and 3.20 V and a single discharge plateau at 2.75 V are clearly distinguished. The voltage plateaus are reflected as redox peaks in the CV curves (Figure 6a). Two charge plateaus (or two oxidative peaks in the CV plot) correspond respectively to a two-phase reaction from $NaFePO_4$ to $Na_{2/3}FePO_4$ and a solid solution reaction from $Na_{2/3}FePO_4$ to $FePO_4$.[32,35,36] One notes that the hysteresis between the charge−discharge voltage plateaus of $NaFePO_4$ is larger than that of $LiFePO_4$ in LIBs (Figure S1a), which might be caused by a higher energy difference during phase transition and slower intercalation kinetics in the olivine framework as well as larger charge transfer resistance for Na ions than for Li ions.[31] The electrode first delivers a reversible capacity of 111 mAh g^{-1} (Figure 6b), which is lower than that (137 mAh g^{-1}) obtained in aqueous electrolyte (Figure 3b) at the same discharge rate, indicating slower reaction kinetics in organic electrolyte due to lower ionic conductivity and higher viscosity of the organic electrolyte compared to in aqueous electrolyte. However, the $NaFePO_4$/C electrode reported here displays higher capacity for Na ion storage in the organic system than most of the previous works.[18,28,31,38] Obviously, the charge profile of the first cycle is different from the subsequent cycles. The different charge profile appearing at the first cycle could be attributed to reconstruction of the surface layer between the material and electrolyte. As is well-known, the reaction interface structures between the material and electrolyte are different in aqueous and organic electrolytes. The surface film structure formed in aqueous electrolyte might be unsuitable for ionic diffusion through the interface during charging/discharging in organic electrolyte, thus leading to a larger polarization in the first cycle in organic electrolyte. Moreover, the $NaFePO_4$/C electrode displays almost overlapped charge−discharge profiles in the subsequent cycles, exhibiting excellent Na ion intercalation/deintercalation reversibility. As is shown in Figure 6c, the

DOI: 10.1021/acsami.5b04691
ACS Appl. Mater. Interfaces 2015, 7, 17977−17984

electrode still attains a reversible capacity of 100 mAh g^{-1} after 240 cycles, corresponding to a capacity retention ratio of 90%. The cycle capability greatly exceeds that of $NaFePO_4$ ever reported, as shown in Table S1. Additionally, the reversible capacity increase (the activation process) in the first 15 cycles is possibly due to a slow infiltration of electrolyte into the interior of the $NaFePO_4$/C microsphere, which creates gradually the electrochemically active interface. A similar increase in capacity during the initial cycles has also been observed for the $LiFePO_4$ materials in previous literature.[45,46] The rate capability of $NaFePO_4$/C was also investigated as displayed in Figure 6d. The electrode achieves discharge capacities of 120, 109, 101, 92, 71, and 46 mAh g^{-1} at the C-rates of 0.05, 0.1, 0.2, 0.5, 1, and 2 C, respectively, which are better than most of the previous reports so far.[28,31]

The preceding test results are indicative of excellent electrochemical reversibility and rate capability of the $NaFePO_4$/C electrode developed in this work, superior to those synthesized by chemical or electrochemical oxidation/reduction reactions in organic solutions started from $LiFePO_4$ precursors. We believe that the aqueous electrochemical displacement method is advantageous owing to the very fast de(intercalation) kinetics of Li and Na ions in the aqueous solution. On this account, Li ions can be fully extracted from the lattice promoted by the potential field even at relatively large current rate. No Li ion residuals in the resulting $FePO_4$ lattice is very crucial to making sure there are more lattice sites and more fluent channels for Na ion intercalation. Fast reaction kinetics also brings about lower potential polarization so as to cause smaller structural deformation. Besides, aqueous solution would create less detriment to the structure of materials. In contrast, the chemical delithiation of $LiFePO_4$ using strong oxidizer such as NO_2BF_4 and bromine was found to create structural defects and amorphization due to the violent reaction.[47,48] Therefore, the aqueous electrochemical displacement method not only provides an effective, easy, cost-saving, and green preparation route for olivine $NaFePO_4$ but also endows desirable electrochemical performance.

3.3. Study on Phase Transition during Electrochemical Reaction. Besides the pursuit of favorable synthesis means and honorable electrochemical performance with the olivine-type metallophosphate family, the scientific community also has particular interest in understanding the fundamental reaction mechanics accompanying the alkali metal de(intercalation). As is commonly observed in the host materials that suffer from huge volume change during de(intercalation), such as anatase TiO_2,[49] some layered intercalation compounds,[50] $LiMnPO_4$ (8.9% difference in unit volume).[51] and even $LiFePO_4$ (only 6.9%),[38] the lattice structures would experience a stage transformation process to buffer the mechanical strain. This staging phenomenon also happens in $NaFePO_4$, due to the large volumetric mismatch between $NaFePO_4$ and $FePO_4$ (ca. 17.58% difference in unit volume). In previous research studies, the formation of an intermediate ordered $Na_{2/3}FePO_4$ superstructure was identified by various spectroscopic techniques,[37,52] composition−temperature phase diagram,[36] and two plateaus on battery charging,[32,35] so that two successive stage phase transformations from $NaFePO_4$ to $Na_{2/3}FePO_4$ and then to $FePO_4$ were reasonably established. However, the voltage profiles on battery discharge in previous observations only showed a single plateau, which was attributed to the fact that phase transformation from $Na_{2/3}FePO_4$ to $NaFePO_4$ (3.6% difference in volume) present much lower kinetic barriers compared to that from $FePO_4$ to $Na_{2/3}FePO_4$ (13.5% difference in volume).[35,38]

In the preceding rate capability experiment, we found an interesting phenomenon wherein a voltage profile evolution occurred with the acceleration of discharge rate. As is shown in Figure 7, the voltage profiles at low discharge rates of 0.05 and

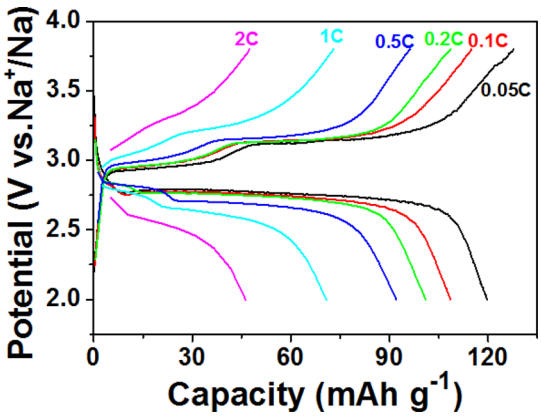

Figure 7. Voltage−capacity profiles of the $NaFePO_4$/C electrode at different charge/discharge rates from 0.05 to 2 C.

0.1 C show only a single discharge plateau, similar to the previous observations. However, as the current rate increases to ≥0.2 C, two distinct plateaus separated by a large voltage gap (0.1 V) appear. The distinct divide of the discharge plateaus indicates that a $Na_{2/3}FePO_4$ intermediate phase also forms upon sodiation process. To confirm the presence of the intermediate phase at high discharge rate, *ex situ* X-ray diffraction (XRD) was employed to characterize the phase transformation during the whole Na ion intercalation process in the $FePO_4$/C electrode. As presented in Figure S2, the XRD diffractions correspond to a $FePO_4$ phase at open circuit voltage. When discharged at 0.5 C to the end of the first voltage plateau around 2.75 V, a set of new XRD diffractions appear pointing out a discharge intermediate of $Na_{2/3}FePO_4$ phase.[32,35,36,52] After full discharge to 2.0 V, all of the $Na_{2/3}FePO_4$ signals disappear again and the diffraction pattern can be indexed to a pure phase of $NaFePO_4$. Thus, the *ex situ* XRD measurement and discharge voltage profile corroborate that Na ion intercalation actually goes through a similar reaction path via a $Na_{2/3}FePO_4$ intermediate phase to the deintercalation process. Additionally, the TEM and selected area electron diffraction (SAED) pattern were also performed to confirm the presence of the $Na_{2/3}FePO_4$ intermediate as shown in Figure 8. The SAED pattern from the TEM images of the intermediate during discharging displayed the diffraction spots obtained along the $[1\bar{1}0]$ direction. Particularly, some superlattice spots (Figure 8a) can be observed apparently in the SAED pattern compared to the $NaFePO_4$ sample (Figure 4c). The superstructure is considered as the contribution of a Na ion pair and Fe^{II}/Fe^{III} charge ordering reported by previous literature, indicating the characteristics of the $Na_{2/3}FePO_4$ intermediate.[37,38,52] Similar to Boucher's study,[37] the superlattice spots disappear after 1 min irradiation (Figure 8b), due to its instability when exposed to electron beam at room temperature. This phenomenon gives strong evidence to prove that the $Na_{2/3}FePO_4$ intermediate is indeed present during discharging. To the best of our knowledge, this is the first direct evidence of two successive stage phase transformation

DOI: 10.1021/acsami.5b04691
ACS Appl. Mater. Interfaces 2015, 7, 17977−17984

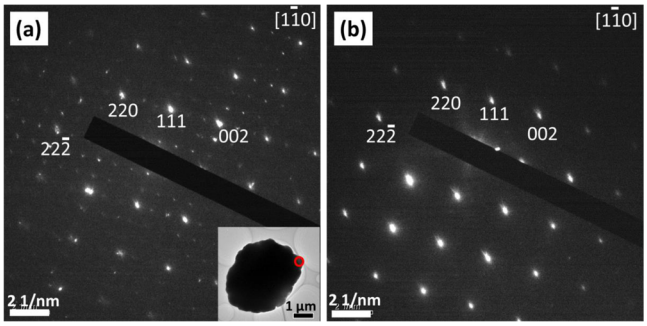

Figure 8. Selected electron diffraction patterns of the $Na_{2/3}FePO_4$ intermediate: (a) pattern obtained along the $[1\bar{1}0]_{Pnma}$ zone axis and (b) same position as a but after 1 min irradiation.

processes during Na ion intercalation into $FePO_4$ by means of constant current discharge. This discovery could adequately resolve the uncertainties in previous studies of whether $Na_{2/3}FePO_4$ intermediate phase is present during discharge.[35,38]

3.4. Electrochemical Mechanism of Olivine $NaFePO_4$.

Since the discharge process is two successive first order phase transformations via $Na_{2/3}FePO_4$ intermediate phase, the reaction can be written as follows:

$$FePO_4 \xrightarrow{k_1} Na_{2/3}FePO_4 \xrightarrow{k_2} NaFePO_4 \quad (1)$$

k_1 and k_2 are the rate constants for the reaction from $FePO_4$ to $Na_{2/3}FePO_4$ and that from $Na_{2/3}FePO_4$ to $NaFePO_4$, respectively. Because the unit volume expansion (13.5%) from $FePO_4$ to $Na_{2/3}FePO_4$ is more than 3 times larger than that (3.6%) from $Na_{2/3}FePO_4$ to $NaFePO_4$, the first phase transformation should overcome a much higher kinetics barrier than the follow-up one; namely, $k_1 \ll k_2$. Therefore, at low reaction rates, $Na_{2/3}FePO_4$ formed from the first transformation process would transform into $NaFePO_4$ immediately. Thus, the apparent reaction looks like a direct transformation from $FePO_4$ to $NaFePO_4$, as reflected by a single voltage plateau on discharge profiles. At high reaction rates otherwise, the high electrochemical overpotential greatly accelerates the first transformation, which becomes even comparative to the subsequent one; the apparent reaction would exhibit a two-step phase transformation, corresponding to two voltage plateaus on the discharge curves. However, it should be addressed that, in the charge process, whether at low or high rates, $NaFePO_4$ would always transform into $Na_{2/3}FePO_4$ at first, which then transforms into $FePO_4$ ($k_2 \gg k_1$), so that the charge would always exhibit a two-step phase transformation process (two voltage plateaus).

To verify the preceding discussion, cyclic voltammetry was reconducted on the $NaFePO_4$/C electrode at high scan rates of 0.5, 1, and 2 mV s^{-1} as presented in Figure 9. As expected, two well-defined reductive peaks emerge at high scan rates compared to one reductive peak at 0.05 mV s^{-1} (Figure 6a). The current peaks in the CV curves are in good accord with the discharge plateaus at high rates (Figure 7). Because cyclic voltammetry is a transient method, it can capture a short-lifetime reaction intermediate by regulating the scan rates. Because k_1 is much smaller than k_2 in eq 1, $Na_{2/3}FePO_4$ would transform into $NaFePO_4$ immediately as soon as it is produced during slow scan. Therefore, the concentration of $Na_{2/3}FePO_4$ intermediate in the system is very low and cannot be captured by CV. As the scan rate expedites, the concentration of the intermediate would accumulate to be detected. Consequently, a

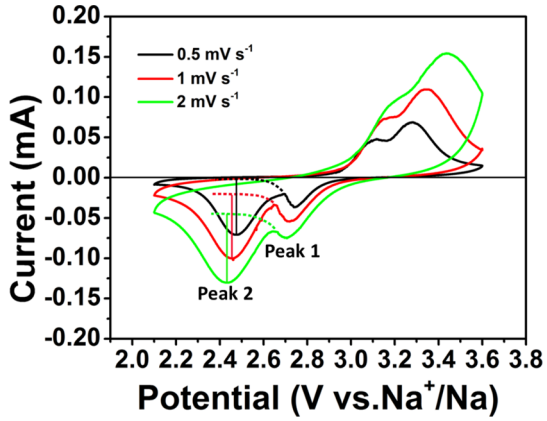

Figure 9. Cyclic voltammograms of $NaFePO_4$/C electrode in 1 mol L^{-1} $NaPF_6$/EC:DEC (1:1 in vol) solution at various scan rates.

reductive peak derived from the fast reaction (k_2) would split away from the primary single peak. Thus, the CV results further verify the existence a $Na_{2/3}FePO_4$ intermediate during Na intercalation process, and a two-step phase transformation process occurs both on Na intercalation and deintercalation. Obviously, this reaction rate dependent $Na_{2/3}FePO_4$ appearance is in fact rooted from the disparity of k_1 and k_2.

According to Bard's book,[53] the peak current i_p has a relationship with the peak potential E_p as displayed by the following equation:

$$i_p = 0.227nFAC_0^*k^0 \exp[-af(E_p - (E^0)')] \quad (2)$$

where $(E^0)'$ is the formal potential for the reduction. For a multistep charge transfer reaction, the peak current (i_p) in the $i-E$ curve is the sum of the individual $i-E$ curves of $FePO_4$ and $Na_{2/3}FePO_4$. In this regards, the measurement of i_{p2} must be made using the decaying current of the first wave as the baseline. The values of i_{p2} are corrected correspondingly as shown in Figure 9, and the related parameters of eq 1 are shown in Table S2.

According to eq 2, a plot of ln i_p vs $E_p - (E^0)'$ determined at different scan rates should have a slope of $-af$ and an intercept proportional to k^0; namely,

$$\ln i_p = -af(E_p - (E^0)') + \ln(0.227nFAC_0^*k) \quad (3)$$

Considering peak 1 and peak 2, we get the different lines as shown in Figure 10. At 25 °C, for F = 96485.4 C mol^{-1}, A is $\pi r^2/6$ = 0.13083 cm^2, C_{10}^* = C_{20}^* = 1 mol L^{-1}, n = 2/3 for k_1 or 1/3 for k_2, and the values of k_1 and k_2 are deduced to be 1.21 × 10^{-6} cm s^{-1} and 2.43 × 10^{-5} cm s^{-1} based on eq 3 and the corresponding intercept obtained from Figure 10, respectively. Clearly, k_2 corresponding to the reaction from $Na_{2/3}FePO_4$ to

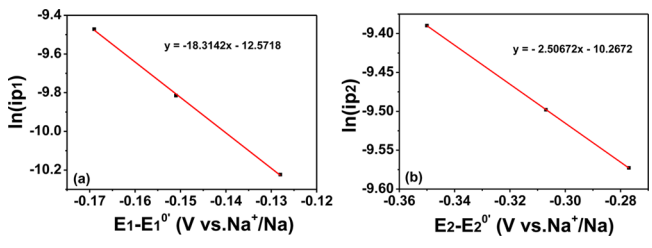

Figure 10. Plot of ln i_{p1} vs $E_{p1} - (E^0_1)'$ (a) and plot of ln i_{p2} vs $E_{p2} - (E_2^0)'$ (b) determined at different scan rates.

DOI: 10.1021/acsami.5b04691
ACS Appl. Mater. Interfaces 2015, 7, 17977−17984

$NaFePO_4$ is about 20-fold higher than k_1 for the reaction from $FePO_4$ to $Na_{2/3}FePO_4$. This result further demonstrates the preceding discussion, which is an identical two-step phase transition reaction upon Na intercalation and deintercalation processes.

4. CONCLUSIONS

In summary, olivine $NaFePO_4$/C cathode was prepared by a facile aqueous electrochemical displacement method from olivine $LiFePO_4$/C precursor. The $NaFePO_4$/C cathode displays a high discharge capacity of 111 mAh g^{-1} along with 90% capacity retention over 240 cycles at 0.1 C and high rate capacity (46 mAh g^{-1} at 2 C). The excellent electrochemical performance demonstrates that the electrochemical displacement method offers an inexpensive, effective, and promising approach to prepare $NaFePO_4$/C materials for Na-based energy storage applications. Of particular significance is that we first observe the appearance of $Na_{2/3}FePO_4$ intermediate during Na intercalation process with conventional electrochemical techniques, corroborating an identical two-step phase transition reaction upon Na intercalation and deintercalation processes. The clarification of the electrochemical reaction mechanism could also inspire more attention on the development of high-performance $NaFePO_4$ material.

■ ASSOCIATED CONTENT

Supporting Information

The Supporting Information is available free of charge on the ACS Publications website at DOI: 10.1021/acsami.5b04691.

Electrochemical characterization of the $LiFePO_4$/C electrode, charge/discharge curves of the $NaFePO_4$/C and corresponding XRD patterns of the $NaFePO_4$/C electrode at different discharge depths, comparison of the cycle performance of the olivine $NaFePO_4$ electrode, and measured and calculated data based on the i–E curves of the $NaFePO_4$/C electrode (PDF).

■ AUTHOR INFORMATION

Corresponding Authors

*(Y.C.) E-mail: ylcao@whu.edu.cn.
*(L.X.) E-mail: lfxiao@mail.ccnu.edu.cn.

Notes

The authors declare no competing financial interest.

■ ACKNOWLEDGMENTS

We are thankful for the financial support by the National Key Basic Research Program of China (Grant No. 2015CB251100) and the National Science Foundation of China (Grant Nos. 21373155 and 21333007).

■ REFERENCES

(1) Zu, C.; Li, H. Thermodynamic Analysis on Energy Densities of Batteries. *Energy Environ. Sci.* **2011**, *4*, 2614–2624.
(2) Slater, M. D.; Kim, D.; Lee, E.; Johnson, C. S. Sodium-Ion Batteries. *Adv. Funct. Mater.* **2013**, *23*, 947–958.
(3) Kim, S.-W.; Seo, D.-H.; Ma, X.; Ceder, G.; Kang, K. Electrode Materials for Rechargeable Sodium-Ion Batteries: Potential Alternatives to Current Lithium-Ion Batteries. *Adv. Energy Mater.* **2012**, *2*, 710–721.
(4) Pan, H.; Hu, Y.; Chen, L. Room-Temperature Stationary Sodium-Ion Batteries for Large-Scale Electric Energy Storage. *Energy Environ. Sci.* **2013**, *6*, 2338–2360.
(5) Luo, W.; Allen, M.; Raju, V.; Ji, X. An Organic Pigment as a High-Performance Cathode for Sodium-Ion Batteries. *Adv. Energy Mater.* **2014**, *4*, 1400554.
(6) Lu, X.; Kirby, B. W.; Xu, W.; Li, G.; Kim, J. Y.; Lemmon, J. P.; Sprenkle, V. L.; Yang, Z. Advanced Intermediate-Temperature Na–S Battery. *Energy Environ. Sci.* **2013**, *6*, 299–306.
(7) Tripathi, R.; Wood, S. M.; Islam, M. S.; Nazar, L. F. Na-Ion Mobility in Layered Na_2FePO_4F and Olivine $Na[Fe,Mn]PO_4$. *Energy Environ. Sci.* **2013**, *6*, 2257–2264.
(8) Hamani, D.; Ati, M.; Tarascon, J.; Rozier, P. Na_xVO_2 as Possible Electrode for Na-Ion Batteries. *Electrochem. Commun.* **2011**, *13*, 938–941.
(9) Yu, H.; Guo, S.; Zhu, Y.; Ishida, M.; Zhou, H. Novel Titanium-Based O3-Type $NaTi_{0.5}Ni_{0.5}O_2$ as a Cathode Material for Sodium Ion Batteries. *Chem. Commun.* **2014**, *50*, 457–459.
(10) Wang, Y.; Yu, X.; Xu, S.; Bai, J.; Xiao, R.; Hu, Y.-S.; Li, H. H.; Yang, X.-G.; Chen, L.; Huang, X. A Zero-Strain Layered Metal Oxide as the Negative Electrode for Long-Life Sodium-Ion Batteries. *Nat. Commun.* **2013**, *4*, 2365.
(11) Yuan, D.; Liang, X.; Wu, L.; Cao, Y.; Ai, X.; Feng, J.; Yang, H. A Honeycomb-Layered $Na_3Ni_2SbO_6$: A High-Rate and Cycle-Stable Cathode for Sodium-Ion Batteries. *Adv. Mater.* **2014**, *26*, 6301–6306.
(12) Li, Z.; Young, D.; Xiang, K.; Carter, W. C.; Chiang, Y. Towards High Power High Energy Aqueous Sodium-Ion Batteries: The $NaTi_2(PO_4)_3/Na_{0.44}MnO_2$ System. *Adv. Energy Mater.* **2013**, *3*, 290–294.
(13) Cao, Y.; Xiao, L.; Wang, W.; Choi, D.; Nie, Z.; Yu, J.; Saraf, L. V.; Yang, Z.; Liu, J. Reversible Sodium Ion Insertion in Single Crystalline Manganese Oxide Nanowires with Long Cycle Life. *Adv. Mater.* **2011**, *23*, 3155–3160.
(14) Jian, Z.; Zhao, L.; Pan, H.; Hu, Y.; Li, H.; Chen, W.; Chen, L. Carbon Coated $Na_3V_2(PO_4)_3$ as Novel Electrode Material for Sodium Ion Batteries. *Electrochem. Commun.* **2012**, *14*, 86–89.
(15) Jian, Z.; Han, W.; Lu, X.; Yang, H.; Hu, Y.; Zhou, J.; Zhou, Z.; Li, J.; Chen, W.; Chen, D.; Chen, L. Superior Electrochemical Performance and Storage Mechanism of $Na_3V_2(PO_4)_3$ Cathode for Room-Temperature Sodium-Ion Batteries. *Adv. Energy Mater.* **2013**, *3*, 156–160.
(16) Saravanan, K.; Mason, C. W.; Rudola, A.; Wong, K. H.; Balaya, P. The First Report on Excellent Cycling Stability and Superior Rate Capability of $Na_3V_2(PO_4)_3$ for Sodium Ion Batteries. *Adv. Energy Mater.* **2013**, *3*, 444–450.
(17) Fang, Y.; Xiao, L.; Qian, J.; Ai, X.; Yang, H.; Cao, Y. Mesoporous Amorphous $FePO_4$ Nanospheres as High-Performance Cathode Material for Sodium-Ion Batteries. *Nano Lett.* **2014**, *14*, 3539–3543.
(18) Zaghib, K.; Trottier, J.; Hovington, P.; Brochu, F.; Guerfi, A.; Mauger, A.; Julien, C. M. Characterization of Na-Based Phosphate as Electrode Materials for Electrochemical Cells. *J. Power Sources* **2011**, *196*, 9612–9617.
(19) Li, S.; Dong, Y.; Xu, L.; Xu, X.; He, L.; Mai, L. Effect of Carbon Matrix Dimensions on the Electrochemical Properties of $Na_3V_2(PO_4)_3$ Nanograins for High-Performance Symmetric Sodium-Ion Batteries. *Adv. Mater.* **2014**, *26*, 3545–3553.
(20) Lee, K. T.; Ramesh, T. N.; Nan, F.; Botton, G.; Nazar, L. F. Topochemical Synthesis of Sodium Metal Phosphate Olivines for Sodium-Ion Batteries. *Chem. Mater.* **2011**, *23*, 3593–3600.
(21) Qian, J.; Zhou, M.; Cao, Y.; Ai, X.; Yang, H. Nanosized $Na_4Fe(CN)_6$/C Composite as a Low-Cost and High-Rate Cathode Material for Sodium-Ion Batteries. *Adv. Energy Mater.* **2012**, *2*, 410–414.
(22) Wang, L.; Lu, Y.; Liu, J.; Xu, M.; Cheng, J.; Zhang, D.; Goodenough, J. B. A Superior Low-cost Cathode for a Na-Ion Battery. *Angew. Chem., Int. Ed.* **2013**, *52*, 1964–1967.
(23) Wessells, C. D.; Peddada, S. V.; Huggins, R. A.; Cui, Y. Nickel Hexacyanoferrate Nanoparticle Electrodes for Aqueous Sodium and Potassium Ion Batteries. *Nano Lett.* **2011**, *11*, 5421–5425.
(24) Zhu, C.; Song, K.; Van Aken, P. A.; Maier, J.; Yu, Y. Carbon-Coated $Na_3V_2(PO_4)_3$ Embedded in Porous Carbon Matrix: An

DOI: 10.1021/acsami.5b04691
ACS Appl. Mater. Interfaces 2015, 7, 17977–17984

Ultrafast Na-Storage Cathode with the Potential of Outperforming Li Cathodes. *Nano Lett.* **2014**, *14*, 2175−2180.
(25) Li, H.; Yu, X.; Bai, Y.; Wu, F.; Wu, C.; Liu, L.; Yang, X. Effects of Mg Doping on the Remarkably Enhanced Electrochemical Performance of $Na_3V_2(PO_4)_3$ Cathode Materials for Sodium Ion Batteries. *J. Mater. Chem. A* **2015**, *3*, 9578−9586.
(26) Li, H.; Bai, Y.; Wu, F.; Li, Y.; Wu, C. Budding Willow Branches Shaped $Na_3V_2(PO_4)_3$/C Nanofibers Synthesized Via an Electrospinning Technique and Used as Cathode Material for Sodium Ion Batteries. *J. Power Sources* **2015**, *273*, 784−792.
(27) Minakshi, M.; Meyrick, D.; Appadoo, D. Maricite ($NaMn_{1/3}Ni_{1/3}Co_{1/3}PO_4$)/Activated Carbon: Hybrid Capacitor. *Energy Fuels* **2013**, *27*, 3516−3522.
(28) Oh, S.-M.; Myung, S.; Hassoun, J.; Scrosati, B.; Sun, Y. Reversible $NaFePO_4$ Electrode for Sodium Secondary Batteries. *Electrochem. Commun.* **2012**, *22*, 149−152.
(29) Zhao, J.; Jian, Z.; Ma, J.; Wang, F.; Hu, Y.; Chen, W.; Chen, L.; Liu, H.; Dai, S. Monodisperse Iron Phosphate Nanospheres: Preparation and Application in Energy Storage. *ChemSusChem* **2012**, *5*, 1495−1500.
(30) Wongittharom, N.; Lee, T.; Wang, C.; Wang, Y.; Chang, J. Electrochemical Performance of Na/$NaFePO_4$ Sodium-Ion Batteries with Ionic Liquid Electrolytes. *J. Mater. Chem. A* **2014**, *2*, 5655−5661.
(31) Zhu, Y.; Xu, Y.; Liu, Y.; Luo, C.; Wang, C. Comparison of Electrochemical Performances of Olivine $NaFePO_4$ in Sodium-Ion Batteries and Olivine $LiFePO_4$ in Lithium-Ion Batteries. *Nanoscale* **2013**, *5*, 780−787.
(32) Moreau, P.; Guyomard, D.; Gaubicher, J.; Boucher, F. Structure and Stability of Sodium Intercalated Phases in Olivine $FePO_4$. *Chem. Mater.* **2010**, *22*, 4126−4128.
(33) Sun, A.; Manivannan, A. Structural Studies on $NaFePO_4$. *J. Electrochem. Soc. Transactions.* **2011**, *35*, 3−7.
(34) Le Poul, N. Development of Potentiometric Ion Sensors Based on Insertion Materials as Sensitive Element. *Solid State Ionics* **2003**, *159*, 149−158.
(35) Galceran, M.; Saurel, D.; Acebedo, B.; Roddatis, V. V.; Martin, E.; Rojo, T.; Casas-Cabanas, M. The Mechanism of $NaFePO_4$ (De)Sodiation Determined by in situ X-Ray Diffraction. *Phys. Chem. Chem. Phys.* **2014**, *16*, 8837−8842.
(36) Lu, J.; Chung, S. C.; Nishimura, S.; Yamada, A. Phase Diagram of Olivine Na_xFePO_4 ($0 < x < 1$). *Chem. Mater.* **2013**, *25*, 4557−4565.
(37) Boucher, F.; Gaubicher, J.; Cuisinier, M.; Guyomard, D.; Moreau, P. Elucidation of the $Na_{2/3}FePO_4$ and $Li_{2/3}FePO_4$ Intermediate Superstructure Revealing a Pseudouniform Ordering in 2D. *J. Am. Chem. Soc.* **2014**, *136*, 9144−9157.
(38) Casas-Cabanas, M.; Roddatis, V. V.; Saurel, D.; Kubiak, P.; Carretero-González, J.; Palomares, V.; Serras, P.; Rojo, T. Crystal Chemistry of Na Insertion/Deinsertion in $FePO_4$−$NaFePO_4$. *J. Mater. Chem.* **2012**, *22*, 17421−17423.
(39) Manjunatha, H.; Venkatesha, T. V.; Suresh, G. S. Kinetics of Electrochemical Insertion of Lithium Ion into $LiFePO_4$ from Aqueous 2M Li_2SO_4 Solution Studied by Potentiostatic Intermittent Titration Technique. *Electrochim. Acta* **2011**, *58*, 247−257.
(40) Vujković, M.; Stojković, I.; Cvjetićanin, N.; Mentus, S. Gel-Combustion Synthesis of $LiFePO_4$/C Composite with Improved Capacity Retention in Aerated Aqueous Electrolyte Solution. *Electrochim. Acta* **2013**, *92*, 248−256.
(41) Wu, X.; Cao, Y.; Ai, X.; Qian, J.; Yang, H. A Low-Cost and Environmentally Benign Aqueous Rechargeable Sodium-Ion Battery Based on $NaTi_2(PO_4)_3$−$Na_2NiFe(CN)_6$ Intercalation Chemistry. *Electrochem. Commun.* **2013**, *31*, 145−148.
(42) Minakshi, M.; Meyrick, D. Reversible Sodiation in Maricite $NaMn_{1/3}Co_{1/3}Ni_{1/3}PO_4$ for Renewable Energy Storage. *J. Alloys Compd.* **2013**, *555*, 10−15.
(43) Vujković, M.; Mentus, S. Fast Sodiation/Desodiation Reactions of Electrochemically Delithiated Olivine $LiFePO_4$ in Aerated Aqueous $NaNO_3$ Solution. *J. Power Sources* **2014**, *247*, 184−188.
(44) Qian, J.; Zhou, M.; Cao, Y.; Ai, X.; Yang, H. Template-Free Hydrothermal Synthesis of Nanoembossed Mesoporous $LiFePO_4$ Microspheres for High-Performance Lithium-Ion Batteries. *J. Phys. Chem. C* **2010**, *114*, 3477−3482.
(45) Wu, X.; Jiang, L.; Cao, F.; Guo, Y.; Wan, L. $LiFePO_4$ Nanoparticles Embedded in a Nanoporous Carbon Matrix Superior Cathode Material for Electrochemical Energy-Storage Devices. *Adv. Mater.* **2009**, *21*, 2710−2714.
(46) Dominko, R.; Goupil, J. M.; Bele, M.; Gaberscek, M.; Remskar, M.; Hanzel, D.; Jamnik, J. Impact of $LiFePO_4$/C Composites Porosity on Their Electrochemical Performance. *J. Electrochem. Soc.* **2005**, *152*, A858−A863.
(47) Chen, G.; Song, X.; Richardson, T. J. Electron Microscopy Study of the $LiFePO_4$ to $FePO_4$ Phase Transition. *Electrochem. Solid-State Lett.* **2006**, *9*, A295−A298.
(48) Jones, J. L.; Hung, J.; Meng, Y. Intermittent X-Ray Diffraction Study of Kinetics of Delithiation in Nano-Scale $LiFePO_4$. *J. Power Sources* **2009**, *189*, 702−705.
(49) Cava, R. J.; Murphy, D. W.; Zahurak, S.; Santoro, A.; Roth, R. S. The Crystal Structures of the Lithium-Inserted Metal Oxides $Li_{0.5}TiO_2$ Anatase, $LiTi_2O_4$ Spinel, and $Li_2Ti_2O_4$. *J. Solid State Chem.* **1984**, *53*, 64−75.
(50) Fernández-Morán, H.; Ohstuki, M.; Hibino, A.; Hough, C. Electron Microscopy and Diffraction of Layered, Superconducting Intercalation Complexes. *Science* **1971**, *174*, 498−500.
(51) Delacourt, C.; Poizot, P.; Morcrette, M.; Tarascon, J.; Masquelier, C. One-Step Low-Temperature Route for the Preparation of Electrochemically Active $LiMnPO_4$ Powders. *Chem. Mater.* **2004**, *16*, 93−99.
(52) Galceran, M.; Roddatis, V.; Zúñiga, F. J.; Pérez-Mato, J. M.; Acebedo, B.; Arenal, R.; Peral, I.; Rojo, T.; Casas-Cabanas, M. Na-Vacancy and Charge Ordering in $Na_{\approx 2/3}FePO_4$. *Chem. Mater.* **2014**, *26*, 3289−3294.
(53) Bard, A. J.; Faulkner, L. R. *Electrochemical Methods: Fundamentals and Applications*, 2nd ed.; Wiley: Hoboken, NJ, USA, 2000.

DOI: 10.1021/acsami.5b04691
ACS Appl. Mater. Interfaces 2015, 7, 17977−17984